Development of the High-performance Bushing Model using Abaqus

Satoshi Ito, Daichi Suzuki, and Masahiro Ueda

Toyota Motor Corporation

***Abstract**: To obtain sufficient accuracy for vehicle dynamic performance simulation, it is necessary to consider bushing amplitude and frequency dependency as well as preload effects in the rubber bushing model. FE models are capable of reproducing these characteristics though it is difficult to obtain sufficient calculation accuracy within practical computation time. This paper proposes a new low DOF bushing model by utilizing the user subroutine functionality of Abaqus. The new bushing model exhibits high computational performance while maintaining precision.*

***Keywords**: Assembly Deformation, Dynamics, Elasticity, Experimental Verification, Hyperelasticity, Multi-Body Dynamics, Plasticity, Rubber, Rubber Bushing, Suspension, Vibration, Viscoelasticity.*

1. Introduction

Ride quality of a vehicle is expressed in terms that directly affect the occupants, such as vibration, noise and harshness (unpleasant sensations such as jolting).Therefore it is considered as a key selling point which determines vehicle performance. Forces which cause these phenomena are transmitted from the engine and powertrain or from the road surface to the vehicle cabin, and thence to the occupants. In order to minimize the level of vibration reaching the cabin, rubber isolators such as engine mounts and suspension bushings are deployed extensively to join the engine and suspension systems to the cabin.

Given that rubber isolators used in the joints between components have a significant bearing on ride quality, the vehicle development process will ideally include a CAE analysis of ride quality including rubber characteristics to provide a preliminary evaluation of ride quality prior to the prototype testing stage. This analysis requires a rubber material model that can accurately reproduce the dynamic characteristics of the rubber, particularly with respect to frequency and amplitude dependency. However, conventional rubber material models that use commercially available structural analysis solvers cannot reproduce both frequency and amplitude dependency at the same time. This makes generation of accurate predictions of transient phenomena such as harshness, where the amplitude is constantly changing, difficult.

The authors have developed a rubber material model [2] (hereafter denoted the “new rubber material model”) based on the nonlinear viscoelastic rubber model proposed by Simo, J.C. [1] that is capable of reproducing both amplitude and frequency dependency which coexist in actual phenomena. The accuracy of the new rubber material model is demonstrated in both quasi-static condition and harmonic oscillation condition. [2]

Bushing components in actual vehicle are generally subjected to simultaneous and transient inputs in the translational as well as rotational directions. It is rare that an input is confined to a specific frequency in a uniaxial direction. At SAE, Hartley, C. et al. (2012) [3] and Nakahara, J. et al. (2015) [4] have previously described methods that are capable of reproducing both frequency and amplitude dependency simultaneously. However these studies tend to concentrate on bushing force generated by inputs in the uniaxial direction. There is no literature on bushing force for multi-axial inputs or transient inputs.

This report aims to improve the accuracy of harshness analysis of a full vehicle. For this purpose, first this study reports on the reproducibility of bushing forces associated with multi-axial inputs and transient inputs in the new rubber material model applied to bushing components in a suspension arm as shown in Figure 1. And next, reports on the new low DOF bushing model.

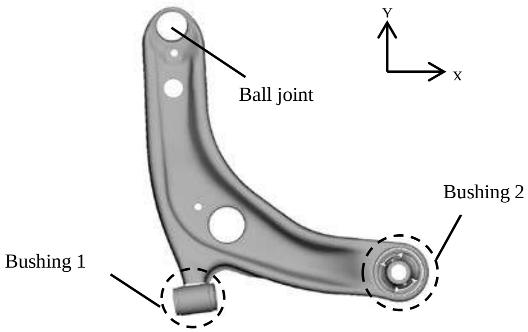

Figure 1. Suspension Arm

2. Rubber material model

2.1 Basic concept of the new rubber material model

Figure 2 illustrates the concept of the rubber material model proposed by Simo, J.C. [1], while Equation 1 shows the associated equation of evolution for stress and strain.

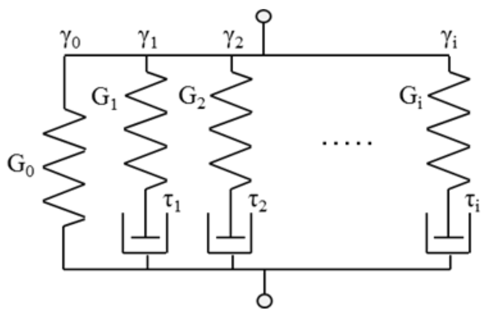

Figure 2. Representation of constitutive law for rubber material

$$\frac{dQ_i}{dt} + \frac{Q_i}{\tau_i} = \frac{\gamma_i}{\tau_i} DEV\left[\frac{2\partial \overline{W}^0(\overline{C})}{\partial \overline{C}}\right] \qquad \text{Equation 1}$$

where

G_i	is the modulus of elasticity for the network
γ_i	is the modulus ratio for the network
τ_i	is relaxation time
Q_i	is stress-like internal variable
$\overline{W}^0$	denotes the deviatoric parts of the initial elastic stored energy
$\overline{C}$	denotes the deviatoric part of the right Cauchy-Green deformation tensor

The new rubber material model describes amplitude dependency by defining relaxation time τ_i in Equation 2 as follows:

$$\tau_i = \frac{1}{A_i}\left|\overline{E}'\right|^{m_i} \qquad \text{Equation 2}$$

where

$\overline{E}'$	is a norm of the strain rate tensor
$A_i \quad m_i$	are material coefficients

Note that these must be identified along with G_i and γ_i in Figure 2. Identification of material coefficients is described below.

2.2 Identification of material coefficients

The network material coefficients were determined from experimental results of test pieces which were manufactured using the material of the bushing components. Figure 3 shows a sample procedure for calculating the material coefficients. The hyperelastic term corresponding to G_0 was modeled with the Yeoh model [5] [6] which is the strain energy per unit of reference volume (the elastic potential that indicates strain energy per unit volume) is expressed as shown in Equation 3.

$$U = \sum_{i=1}^{3} C_{i0}\left(\overline{I}_1 - 3\right)^i + \sum_{i=1}^{3} \frac{1}{D_i}\left(J_{el} - 1\right)^{2i} \qquad \text{Equation 3}$$

where

$\overline{I}_1$ is the first deviatoric strain invariant

J_{el} is the elastic volume ratio

In the Yeoh model, the coefficients of elastic behavior C_{10}, C_{20} and C_{30} are determined from the uniaxial tensile test results, while the coefficient for volumetric change D_i assumes linear volumetric change and is defined for D_1 only. The G_0 value is used for G_1 through G_i. Next, the results from the harmonic oscillation test were used to determine the values of mi and A_i. The proportion of γ_i in each network was determined via optimization with the storage modulus and loss modulus from the harmonic oscillation test which was used as the objective function. Table 1 lists the resulting material coefficients.

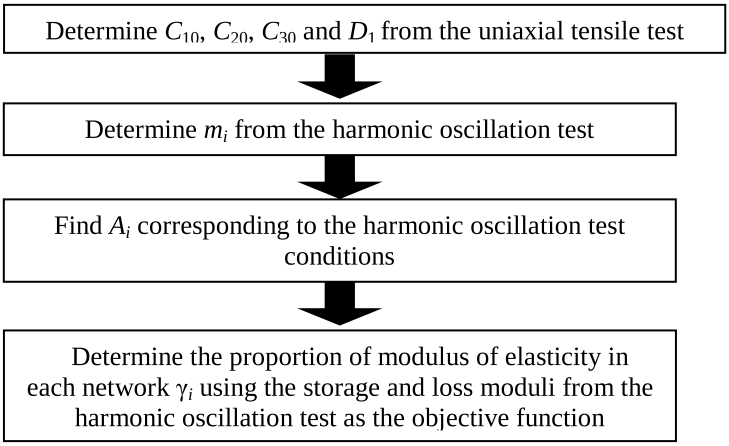

Figure 3. Calculating the material coefficients

Table 1. The material coefficients

	Bushing 1				Bushing 2			
Hyperelasticity parameters	C1	C2	C3	D1	C1	C2	C3	D1
	5.4413	-0.6388	0.2475	0.01	4.403	-0.014	0.269	0.01
Viscoelasticity parameters	Network No.	Ai	γi	mi	Network No.	Ai	γi	mi
	0	—	0.1000	0.897	0	—	0.1000	0.790
	1	10	0.0989		1	10	0.1795	
	2	100	0.0743		2	100	0.1857	
	3	10000	0.3525		3	500	0.2865	
	4	50000	0.3744		4	50000	0.2483	

2.3 Validation of material coefficients

This section shows the validation of material coefficients derived using the procedure detailed above. We used the Abaqus [6] 6-14.1 solver for calculation, and figure 4 shows the single-element validation model used to define the material coefficients thus obtained.

The details are left out on account of the space, though can be referred in [7] .

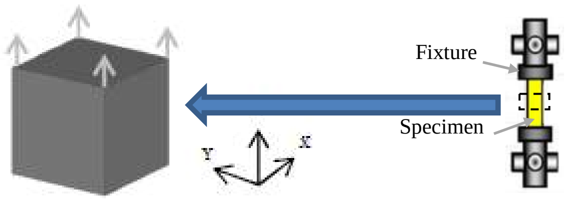

Figure 4. Material test piece model

3. Suspension arm validation

3.1 Suspension arm model

This section describes the suspension arm assembly model used for validation. A bushing model, using the material coefficient validated above was, incorporated into the suspension arm model shown in Figure 5 and used for the purpose of accuracy validation when subjected to transient inputs. A conventional bushing model (see Figure 6) was also created for comparison.

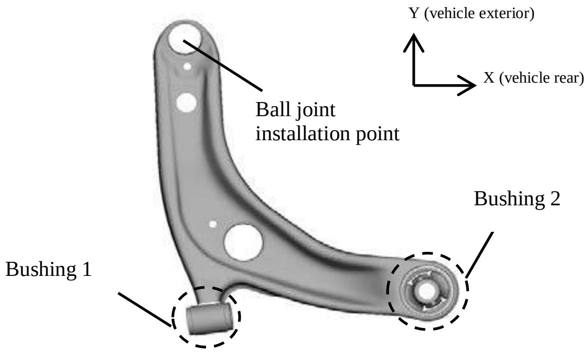

Model specifications

■Elements
Arm: Shell
Rubber: Solid
Internal/external cylinders: Solid
■Model scale
Nodes: 110,270
Elements: 93,818

Figure5. Suspension arm model

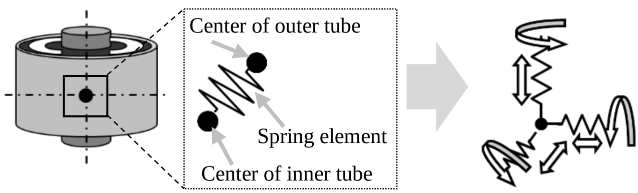

Figure6. Conventional bushing model

3.2 Validation testing

For validation testing, jigs were attached to bushings 1 and 2 as shown in Figures 7 and 8, and displacement input was applied in the vicinity of the ball joint. Figure 8 shows the original position of the suspension arm (unloaded). In the suspension arm test, the initial position of the ball joint set was higher in the Z direction than the original position of suspension arm, as shown in Figure 8, in order to emulate the state of a loaded vehicle. The inputs were a time-series waveform designed to replicate harshness.

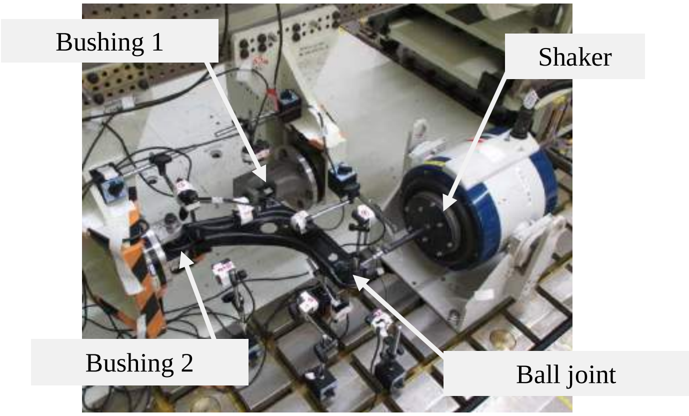

Figure7. Experimental setup

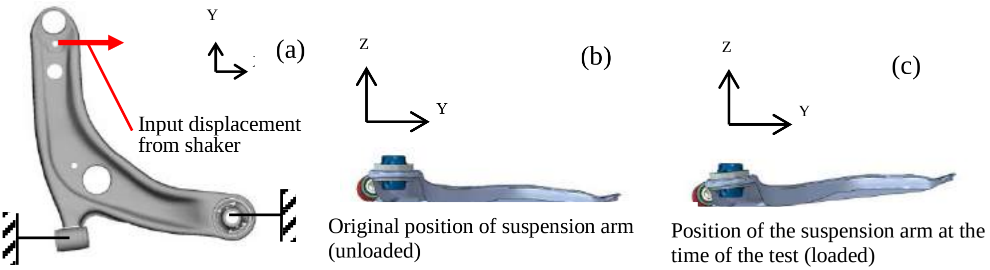

Figure8. Constraint conditions and input position

3.3 Accuracy validation for transient inputs

The compliance of the suspension arm in the vehicle X-direction is controlled by bushing 2. Thus the force in bushing 2 has a significant effect on ride quality. The validation results will be shown in this section by focusing on the force –displacement relation of bushing2, particularly in the X and Y directions of bushing 2.

Figures 7 and 8 illustrate the validation experiments. A shaker was used to impart transient inputs in the vicinity of the ball joint. The displacement waveform at the excitation point was determined from the experiments (see Figure 9) and was also used for the calculation model.

Figure 10 shows bushing displacement in the X direction and Figure 11 compares bushing force in the X direction. It can be seen that the new rubber material model is capable to reproduce the bushing displacement and force waveforms more accurately than the conventional model. In particular the level of the peak which can be seen in test results at t=0.2sec has better correlation when compared to the conventional model. Figure 12 shows bushing displacement in the Y direction and Figure 13 shows bushing force in the Y direction. Once again, the new rubber material model provides excellent reproduction of experimental results in the Y direction.

There are two main reasons which make the new rubber material significantly better for reproducing transient input experiment results. First, as the model is able to reproduce frequency and amplitude dependency simultaneously, it is capable to improve the accuracy when the bushing is subjected to forces such as the experimental conditions shown in Figure 9, where the amplitude is constantly varying. Second, it can reproduce bushing spring characteristics when initial conditions, which are a result of translational displacement, need to be considered (as per Figure 8-(c)).

As a result the new rubber material model is capable to capture the transient characteristics of the bushing forces generated by the displacement inputs acting on the suspension arm.

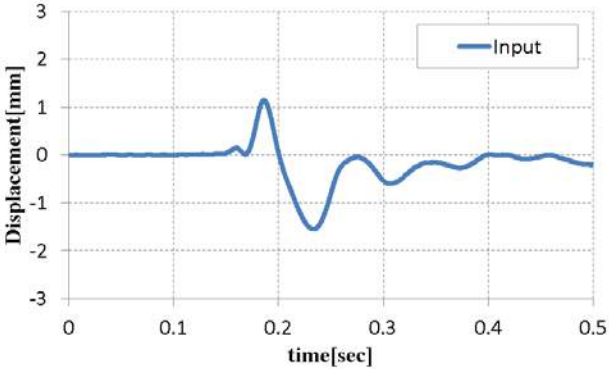

Figure9. Input displacement

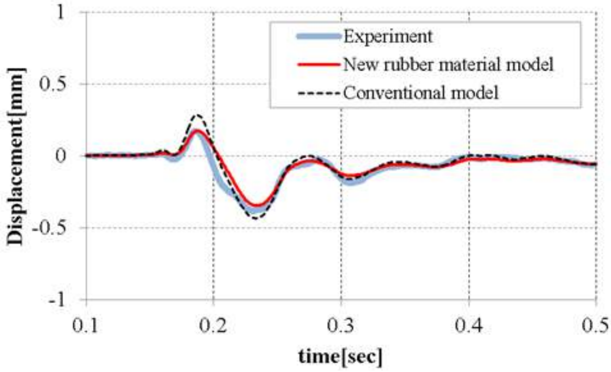

Figure10. Displacement of bushing 2 in the X direction

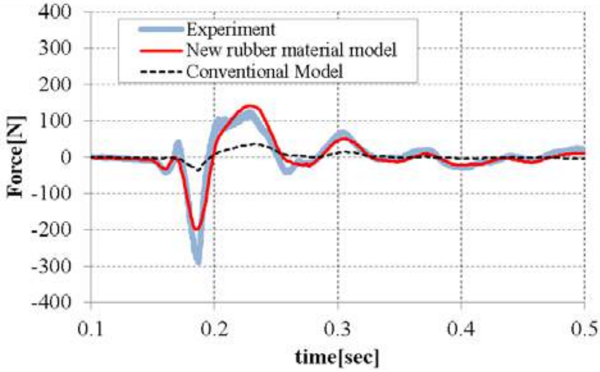

Figure11. Force of bushing 2 in the X direction

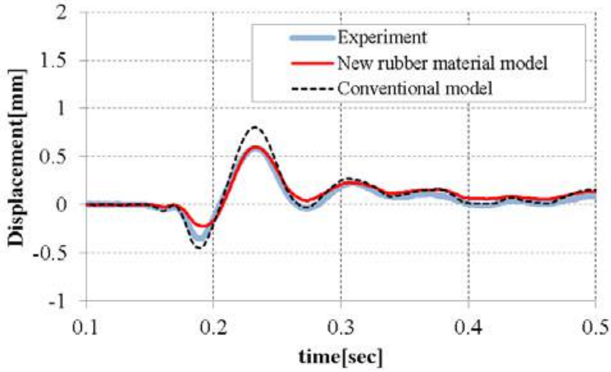

Figure12. Displacement of bushing 2 in the Y direction

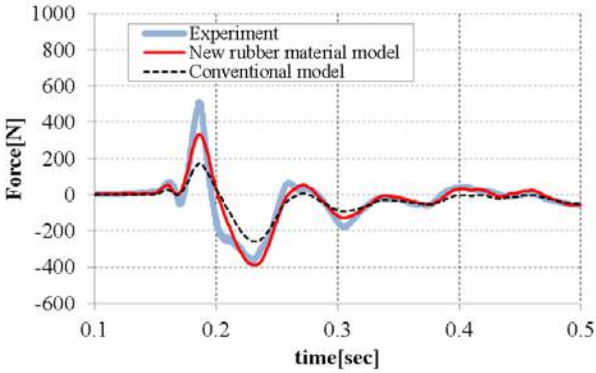

Figure13. Force of bushing 2 in the Y direction

4. New Low DOF Bushing Model

FE models are capable to capture complex characteristics such as amplitude and frequency dependency, though it is difficult to obtain sufficient accuracy within practical computation time. To utilize the developed bushing model for practical application from this section we propose a new low DOF bushing model which has the ability to reproduce these characteristics based on a nonlinear viscoelastic constitutive model of rubber materials .The proposed model is shown in Fig.14.

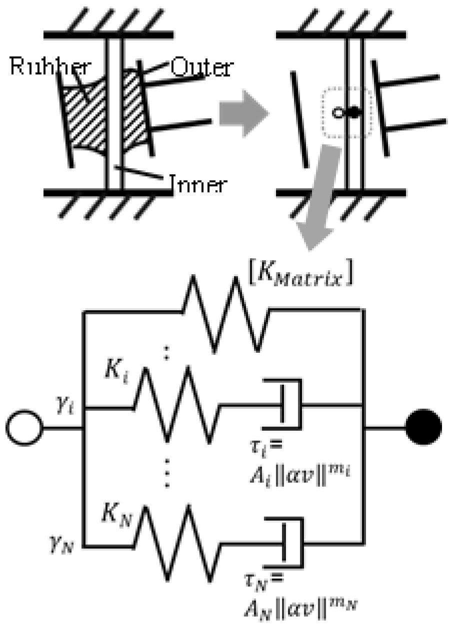

Figure14. Schematic of proposed model

The proposed model provides a bushing-like connection between two nodes. Reaction forces generated in the bushing are calculated by Equation4.

$$\{F\} = \{F^{(h)}\} + \left\{\sum_{i=1}^{N} F_i^{(v)}\right\} \qquad \text{Equation4}$$

where, $\{F\}$ is the total reaction forces, $\{F^{(h)}\}$ is the static reaction forces generated in the spring element, $\{F_i^{(v)}\}$ is the dynamic reaction forces generated in the spring-dashpot model. $\{F^{(h)}\}$ is expressed as shown in Equation5.

$$\{F^{(h)}\} = \sum_{k=1}^{D_S} [K_{Sk}]\{U^k\} + \sum_{k=1}^{D_M} [K_{Mk}]\{(U|U|)^k\} \qquad \text{Equation5}$$

where, $[K_{Sk}]$ and $[K_{Mk}]$ are matrix coefficients, D_S and D_M are polynomial order, U is the relative displacement. The 1st term on the right side of Equation5 represents the reaction forces when preload does not exist. The 2nd term represents the incremental reaction forces due to preload effect. which is expressed in Equation6.

$$F_i^{(v)} = K_i \int_0^t \exp\left(-\frac{t-s}{\tau_i} \right) \dot{U}(s)ds \qquad \text{Equation6}$$

where, τ_i is the relaxation time, and K_i is the spring stiffness. τ_i and K_i is expressed as shown in Equation7,8.

$$\tau_i = A_i \left\| v\alpha \right\|^{m_i} \qquad \text{Equation7}$$

$$K_i = \gamma_i K_{matrix} \qquad \text{Equation8}$$

where, A_i, m_i, γ_i are rubber material coefficients, v is the relative velocity,

is a coefficient determined by the bushing shape, K_{matrix} is the spring stiffness obtained by solving Equation5.

5. Calculation of the matrix coefficient

The calculation of the K_{matrix} used in Equation 5 was obtained by following the procedure .Using a FE model, we calculate the relations between the displacement and reaction forces when subjected to loads from various directions as shown in figure 15.

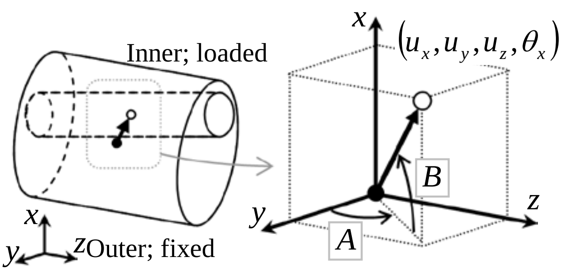

Figure15. Multi-axial loading

Table 1 is a result of the 1550 patterns which was calculated.

Table 2. FEmodel simulation patterns.

a) Pre-rotational angle
θ_x = ±3.75°, ±7.5°, ±11.25°, ±15°
θ_y = ±3.75°, ±7.5°, ±11.25°, ±15°
θ_z = ±3.75°, ±7.5°, ±11.25°, ±15°
$\theta_x = \theta_y = \theta_z$ =0°
25 patterns

b) Translation load direction (62 patterns)

A \ B	-90°	-60°	~	+60°	+90°
0°					
30°	–				–
~	–				–
300°	–				–
330°	–				–

25 × 62 = **1550 patterns**

From the reaction force of the 6 directions characterizing the bushing stiffness and corresponding displacement, we find Ksk by line operation using least-squares method.

6. Process for estimating dynamic coefficients

Process for estimating dynamic coefficients are shown in figure 16.

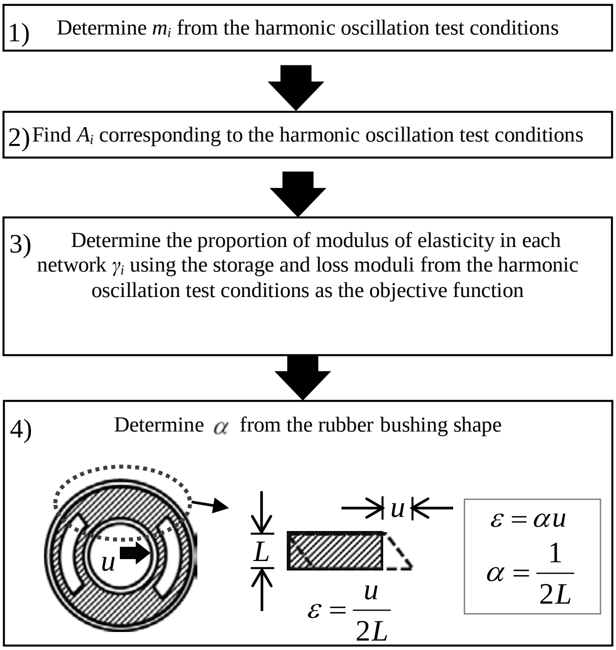

Figure16. Process for estimating dynamic coefficients

7. Validation of rubber bushing component

This section focuses on the validation of the low DOF bushing model by applying it to an actual single rubber bushing component. The bushing shape that we used for validation is shown in figure 17

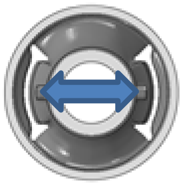

Test conditions Transient

Figure17. Bushing shape

The transient displacement used as input is shown in figure 18

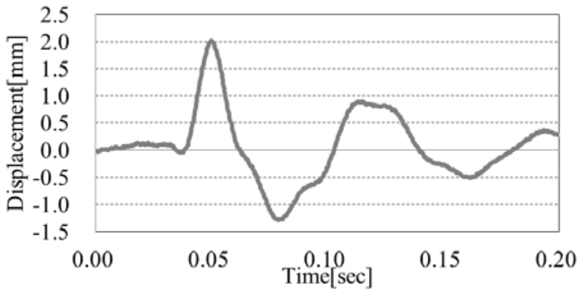

Figure18. Input transient displacement

Results of reaction forces are shown in figure 19 and figure 20 which are in good agreement with experiment.

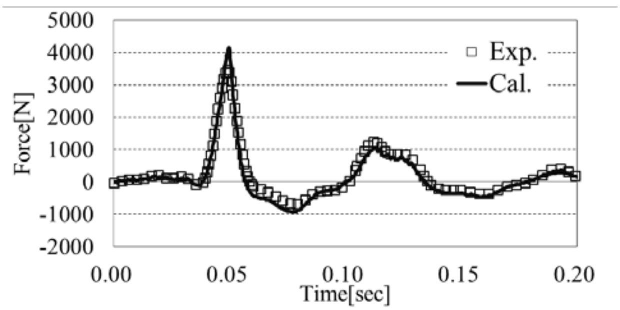

Figure19 . Comparison of dynamic force of bushing in transient

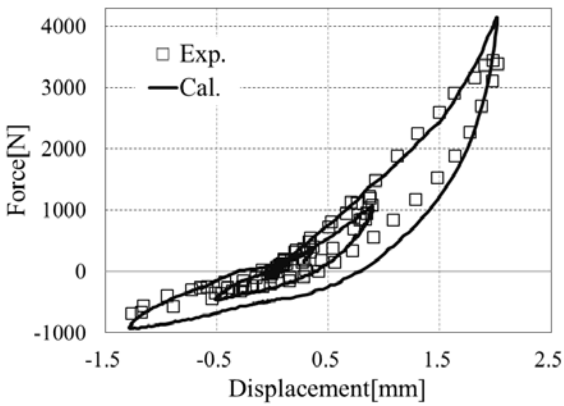

Figure20. Comparison of dynamic hysteresis of bushing in transient

8. Validation of front suspension model

In this section the low DOF bushing model is incorporated into a front suspension model shown in figure 21 for validation. The tire and lower arm was a FE model and the bushing developed in the previous section is encircled in the figure.

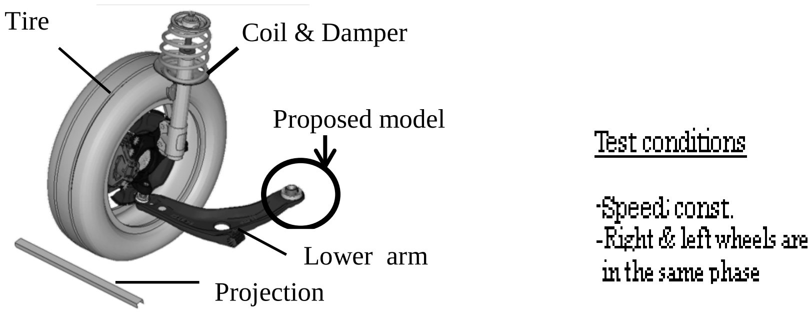

Figure21. Front suspension model

In figure 22, the results of reaction force in the longitudinal direction of the bushing when riding over an obstacle, is shown. The solid line indicates the proposed model and the dotted line indicates the result of a conventional model which is composed by 6springs considering the nonlinear stiffness of the bushing Reaction force of the proposed model corresponds well with experimental results. Figure 23 is a result of frequency analysis of figure22.

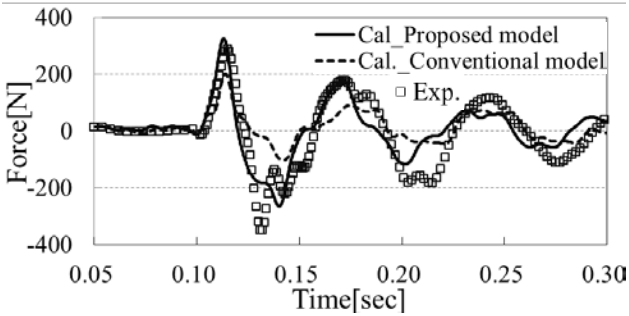

Figure22. Comparison of dynamic force

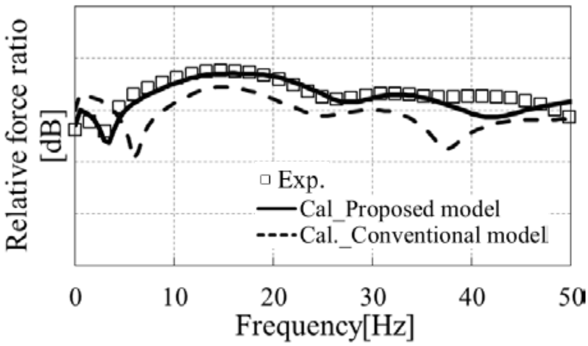

Figure23. Comparison of dynamic force observed by the frequency axis

To confirm the computation cost of the proposed model, the CPU time of the FE model described in section 3 and the proposed low DOF model shown in section 4 is compared in Figure24.The computation time of the low DOF model was 1/3 of the FE model. Using a low DOF tire model (such as F tire), which was a FE model in this comparison further reduction of computation time can be expected.

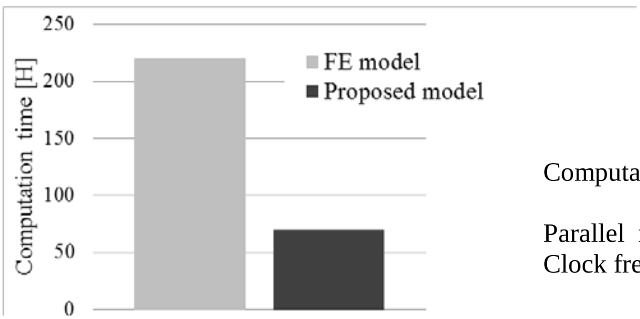

Computation environment

Parallel number 16CPU
Clock frequency 3.3GHz

Figure24. Comparison of computation time

9. Summary

This paper has given an overview of the new rubber material model, together with examples of the procedure for finding the material coefficients of bushings 2. The material coefficients were used to validate the quasi-static uniaxial tensile characteristics and harmonic oscillation characteristics for the material test piece model, as well as static characteristics, harmonic oscillation characteristics and transient characteristics for a stand-alone bushing model. The results demonstrated that a bushing model featuring the new rubber material model can be used to reproduce quasi-static characteristics as well as frequency and amplitude dependency.

The stand-alone bushing model was incorporated into a suspension arm model, which was used to validate the bushing displacement and reaction force through experiments involving harmonic oscillation and transient displacement inputs acting on the suspension arm. The results demonstrated that the new rubber material model is capable of reproducing changes in bushing rigidity caused by multi-axial inputs as well as nonlinear bushing characteristics caused by phenomena such as void contact.

Also by applying the method to calculate K_{matrix} from the FE model shown in section5, a low DOF bushing model with similar accuracy and capable to be simulated within practical computation time was developed. By incorporating this model into a full vehicle simulation where numerous bushings are needed to be considered, simulation can be performed within practical computation time.

10. References

1. Simo, J.C.: On a fully three dimensional finite-strain viscoelastic damage model :Formulation and computational aspects [J], Computer Methods in Applied Mechanics and Engineering, 1987, 60: 153-173
2. Long, Phan Vinh., Satoshi, Ito., Kouhei, Shintani.: A nonlinear viscoelastic constitutive model for dynamic behaviors of rubber FISITA 2014 World Automotive Congress, F2014-IVC-006
3. Hartley, C. and Choi, J.: Finite Element Overlay Technique for Predicting the Payne Effect in a Filled-Rubber Cab Mount, SAE Int. J. Passeng. Cars-Mech. Syst, 2012, 5(1): 413-424
4. Nakahara, J., Yamazaki, K. and Otaki, Y.: Rubber Bushing Model for Vehicle Dynamics Performance Development that Considers Amplitude and Frequency Dependency, SAE Int. 2015-01-1579
5. Marckmann , G. and Verron, E.: Comparison of hyperelastic models for rubber-like materials, Rubber Chemistry and Technology Vol.79(5), 2006, 835-858
6. . Dassault Systemes Simulia Corp.: Abaqus User Manual
7. Masahiro,U.,Daichi,S. and Satoshi,I : Application Study of Nonlinear Viscoelastic Constitutive Model for Dynamic Behavior of Suspension Arm Bushing ,SAE Int.2016-01-1375

11. Acknowledgment

The authors would like to extent their sincere appreciation to everyone who helped review and correct the paper to make it better.